*Journal of Nano- and Electronic Physics*
Vol. **15** No 2, 02021(7pp) (2023)

*Журнал нано- та електронної фізики*
Том **15** № 2, 02021(7cc) (2023)

# A Comprehensive Investigation on Optical and Magnetic Properties of $(In_{1-x}Dy_x)_2O_3$ Nano Powders Prepared by Solid State Reaction Method

Lakshmi Rajesh Chebrolu[1], Madhusudhana Rao Nasina[1,*], Kaleemulla Shaik[2], Maddikera Kalyan Chakravarthi[3]

[1] *Department of Physics, School of Advanced Sciences, VIT-AP University, Amaravati, 522237 Andhra Pradesh, India*
[2] *Thin Films Laboratory, Centre for Functional Materials, Vellore Institute of Technology, Vellore, 632014 Tamil Nadu, India*
[3] *School of Electronics Engineering, VIT-AP University, Amaravati, 522237 Andhra Pradesh, India*

(Received 04 February 2023; revised manuscript received 18 April 2023; published online 27 April 2023)

In this investigation, Dy doped $In_2O_3$ nanoparticles were synthesized using solid-state reaction with different concentrations of 2 at.%, 5 at.%, and 9 at.%. From the X-ray diffraction studies, it was observed the powder samples have a cubic bixbyite crystal structure, and crystallites size was in the range of 31 nm to 82 nm. From the scanning electron microscope images, grain size it was measured and it was in the range of 100 nm to 300 nm. The energy dispersive analysis of X-ray (EDAX) spectra revealed that the synthesized nanoparticles are free from impurities. Using diffuse reflectance spectra, the optical band gap was calculated and it increased from 2.89 eV to 2.96 eV with increase of $Dy^{3+}$ ions concentration. Photoluminescence spectra shown emission peaks in the visible region of the spectrum when samples were excited with a light source of wavelength 410 nm. At ambient temperature, the pure $In_2O_3$ exhibited paramagnetic nature whereas $(In_{1-x}Dy_x)_2O_3$ nanoparticles shown ferromagnetism.

**Keywords:** Indium oxide, Dysprosium oxide, Rare-earth oxides, Solid-state method, Photoluminescence, Vibrating sample magnetometer.

DOI: 10.21272/jnep.15(2).02021 PACS numbers: 77.84.Bw, 78.55.Mb

## 1. INTRODUCTION

Dilute magnetic semiconductors (DMS) find their potential applications in developing of spintronic devices and they play an important role in developing in most advanced future electronic devices such as nano electronic devices. Generally, the semiconductors that exhibit ferromagnetism at room temperature by doping a small quantity of impurity elements such as transition metal ions or magnetic ions [1-3] are considered as dilute magnetic semiconductors. The wide band gap oxide semiconductors such as $In_2O_3$, $SnO_2$, $TiO_2$ and ZnO shown ferromagnetism when they are doped by a small quantity of impurities [4, 5]. Among the different oxide semiconductors, $In_2O_3$ is the promising semiconductor that possess peculiar properties that will be highly useful in many electronic device applications such as magneto resistance, gas sensors, touch screens, liquid crystal displays, transparent conducting electrodes, photo diodes, photo catalysis, ultraviolet lasers, and others [6-9].

Indium oxide ($In_2O_3$) is a transparent conducting oxide material that exhibit electrical conductivity, high optical transparency in the visible range, good thermal and chemical stabilities [10]. Further, indium oxide shows high optical transparency in infrared region, possess wide band gap (3.5 eV) and it is considered as an n-type metal oxide semiconductor [11, 12]. The stoichiometry and high doping limits in $In_2O_3$ play an important role in tuning the optoelectronic properties of indium oxide.

The oxygen vacancy plays a great role in inducing ferromagnetism in $In_2O_3$ along with concentration of impurity ions. With increase in impurity concentration, the carrier concentration can be increased and it may cause to develop oxygen vacancies [13]. Doping rare earth elements in indium oxide ($In_2O_3$) can cause improvement in structural, optical, magnetic, and sensing capabilities of $In_2O_3$ [14-17]. The rare elements such as Eu, Gd, Tm, Yb, Dy, and Nd can be doped in $In_2O_3$ and can improve the physical properties. In order to improve the luminescence efficiency of semiconductors via the energy transfer process, which is more significant from a theoretical and technical point of view, rare earth ions like $Eu^{3+}$, $Dy^{3+}$, and $Er^{3+}$ are added to the semiconductors [18]. Dysprosium oxide ($Dy_2O_3$), is both a rare earth oxide and a basic metal oxide. It is a powder in white in colour, very stable, insoluble, paramagnetic, and slightly hygroscopic. Dysprosium oxide find in applications such as ceramics, glass, lasers, and halide lamps, etc. The manner in which it is prepared has a significant impact on the qualities it possesses [19]. For specialised alloying applications, stainless steel will be supplemented with metals that have a high melting point of dysprosium (2300 °C, $Dy_2O_3$). Further, these materials are used in lasers sources and nuclear controllers.

Hosamani et al. [20] have synthesised Dy-doped $In_2O_3$ by auto combustion procedure and reported ferromagnetic nature [20]. Anand et al. [21] have prepared $Dy^{3+}$: $In_2O_3$ nanoparticles using co-precipitation method for gas sensing applications. In the present study, Dy doped $In_2O_3$ nanoparticles were prepared using simple, low-cost solid-state reaction and studied the role of Dy on structural, morphological, optical, photo luminescent and magnetic properties of $In_2O_3$.

* drnmrao@gmail.com

 

## 2. EXPERIMENTAL METHODS

### 2.1 Sample Preparation

The $(In_{1-x}Dy_x)_2O_3$ nano powders with varied Dy concentrations were synthesised using a solid-state reaction. Powders of indium oxide ($In_2O_3$) and dysprosium oxide ($Dy_2O_3$), were procured from Sigma Aldrich (India) and containing 99.99 % pure trace metals. These two powders were weighed using high accurate microbalance with different $Dy^{3+}$ concentrations such as 0 at.%, 2 at.%, 5 at.%, and 9 at.%. The samples were represented as pure $In_2O_3$, S-X (2 at.%), S-Y (5 at.%), and S-Z (9 at.%). These powders were properly mixed and continued grinding for at 16 hours using Agate mortar and Pestle. These ground powders were calcined in the air for 9 hours at 900 °C using a programmable tubular furnace. The resulting powder samples were cooled to room temperature and the resultant powder exhibited a light yellow after the calcination. The structural, optical, and magnetic characteristics of the synthesized powders were characterized by a variety of characterisation tools and techniques.

### 2.2 Characterization Instruments

X-ray diffractometer (D8 Advance, BRUKER) was used to analyse the structural aspects of $In_2O_3$ such as crystal structure, orientation, and lattice parameters. The surface and elemental analysis of the nanoparticles were studied using field emission scanning electron microscope (FE-SEM) attached with energy dispersive analysis (EDS) (Oxford manufacture Inca Penta FETX3 EDS attachment in Carl Zeiss EVO MA 15 SEM). The optical reflectance and absorbance were recorded in the range of 200 nm to 1100 nm using UV-Vis-spectrophotometer (Lambda 365 Spectrophotometer, PerkinElmer). Photoluminescence spectra of the nanoparticles were recorded using PL spectrophotometer (HORIBA FL-1000). The magnetic properties of the nanoparticles such as magnetization, coercive field, and retentivity were studied using vibrating sample magnetometer (VSM).

## 3. RESULTS AND DISCUSSION

### 3.1 Structural Properties

X-ray diffraction patterns of $(In_{1-x}Dy_x)_2O_3$ nanocrystalline powders at different Dy compositions ($x = 0$, 0.02, 0.05, and 0.09) are shown in Fig. 1. From the figure, it is clear that synthesized nanoparticles exhibit crystallinity. All the diffraction peaks were indexed with planes and found that all these planes were perfectly coincided with cubic structure with an Ia-3 space group (JCPDS Card No: 06-0416). No other diffraction peak related to impurity element Dy was found in XRD patterns indicating the purity of the synthesized nanoparticles. With increase of Dy concentration, a shift in diffraction peaks was observed towards lower diffraction angle ($2\theta$) in XRD patterns. It may be due to difference in ionic radius of $In^{3+}$ and $Dy^{3+}$. It seems that Dy ions replaces In ions as $In^{3+}$, has an ionic radius of 94 pm and the $Dy^{3+}$ has an ionic radius of 91 pm. This shift in diffraction peak was observed when Dy concentration increased from 0 at.% to 9 at.%.

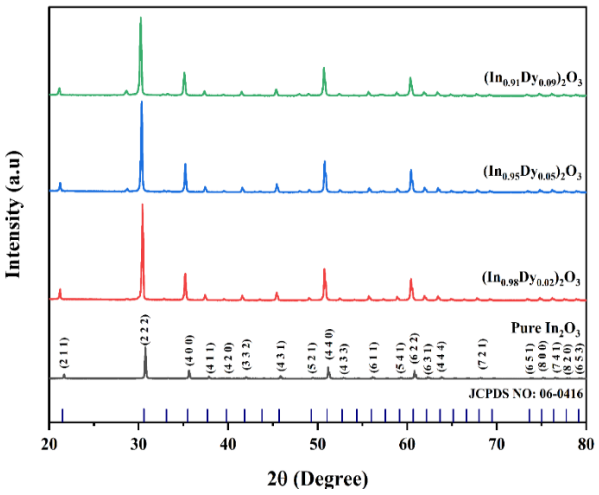


**Fig. 1** – XRD patterns of $(In_{1-x}Dy_x)_2O_3$ nano powders at $x = 0.00$, 0.02, 0.05 and 0.09

From the XRD patterns, it is clear that (222) orientation is dominant which indicates the cubic structure. The (222) peak became broader with increasing Dy concentration and it clearly depicts the increase in full width half maximum (FWHM) and which in turn decreases crystallite size. Similar results were also observed by Anand et al. [12] in Er doped $In_2O_3$ nanoparticles. The crystallite size was calculated using Scherrer equation. The micro strain, dislocation density and lattice parameters of the Dy doped $In_2O_3$ nanoparticles were also calculated and tabulated in Table 1. Fig. 2 shows the XRD patterns of Dy:$In_2O_3$ nanoparticles in the diffraction angle range of 29.8° to 31° and it clearly indicates the shift in (222) peak with increase of Dy concentration. Further, the intensity of the diffraction peak decreased with increase of Dy concentration which indicate that Dy impurity reduces the growth of the crystallite size [22].

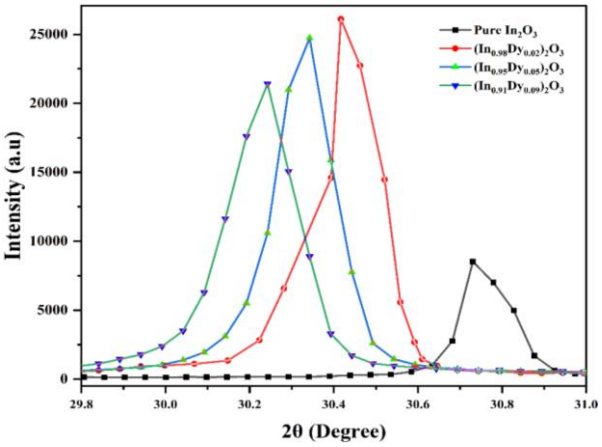


**Fig. 2** – Variation of XRD peak profile (222) of $(In_{1-x}Dy_x)_2O_3$ nano powders with $x = 0.00$, 0.02, 0.05 and 0.09 samples in the diffraction angle $2\theta$ range between 29.8° to 31°

Pure $In_2O_3$ had lattice parameters of 10.06 Å; however, as the amount of dysprosium concentration added to the material increases, the lattice constant increases from 10.16 Å to 10.22 Å as a result of the distortion caused by the substitution of Dy atoms to the host lattice. This occurs because the addition of Dy atoms causes the host lattice to become more distorted. Hosamani et

al. [20] synthesised $(In_{1-x}Dy_x)_2O_3$ nano powder by auto combustion method at a temperature of 400 °C. While doing so, they observed changes in the lattice parameters, that varied from 10.04 Å to 10.11 Å. Using Vegard's rule, a comparison was made between the theoretical and experimental data about the lattice constant, and the results are shown in Fig. 3. When theoretical and practical calculations were compared, it was found that the lattice constant was less for pure $In_2O_3$, and that the lattice constant increased linearly as the concentration of $Dy^{3+}$ atoms increased in $In_2O_3$ (JCPDS Card No: 79-1722).

### 3.2 Morphological Studies

As shown in Fig. 4, the morphological and elemental composition of synthesised nanoparticles were analysed using FESEM in conjunction with EDAX.

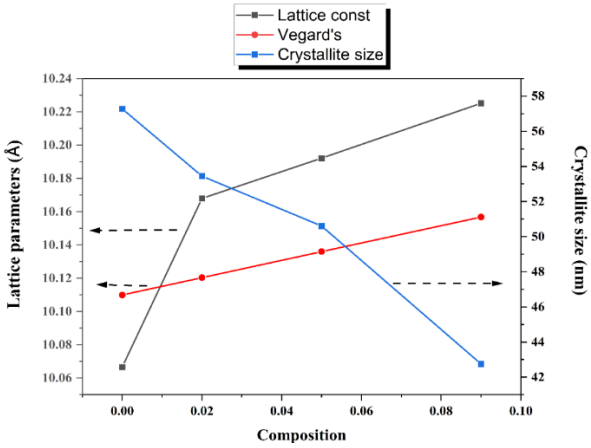


**Fig. 3** – Variation of lattice parameters and crystallite size with Dy ions compositions in prepared $(In_{1-x}Dy_x)_2O_3$ nano powder samples

**Table 1** – Comparison of structural parameters of $(In_{1-x}Dy_x)_2O_3$ nano powder samples from XRD analysis

| $(In_{1-x}Dy_x)_2O_3$ | $2\theta$ (degree) | FWHM '$\beta$' (degree) | Crystallite Size $D$ (nm) | Micro Strain ($10^{-3}$ m) | Dislocation Density ($10^{-14}$ m) | Lattice Constant '$a$' (Å) |
|---|---|---|---|---|---|---|
| $x = 0.00$ | 30.73 | 0.14384 | 57 | 2.28 | 3.048 | 10.06 |
| $x = 0.02$ | 30.41 | 0.15402 | 53 | 2.47 | 3.500 | 10.16 |
| $x = 0.05$ | 30.34 | 0.16265 | 50 | 2.62 | 3.904 | 10.19 |

According to the EDAX spectra, the elemental composition of $(In_{1-x}Dy_x)_2O_3$ with different compositions such as $x = 0.02$, 0.05, and 0.09 demonstrates that it is near to the composition of In, Dy, and O that of target material. Only the peaks for indium, dysprosium, and oxygen were identified in the EDAS spectra. This indicates that the absence of any additional elements. The concentrations of indium, dysprosium, and oxygen atomic percent for different Dy concentration in the $(In_{1-x}Dy_x)_2O_3$ are described in Table 2.

Images obtained using a FESEM show that the $(In_{1-x}Dy_x)_2O_3$ nano powders have semi-spherical and polygonal-shaped particles and are in submicron in size. The particles came together and formed tightly packed structure. The histogram of the $(In_{1-x}Dy_x)_2O_3$ nano powder samples is shown in Fig. 5 with the concentration of Dy ions varied at $x = 0.02$, 0.05, and 0.09. From the

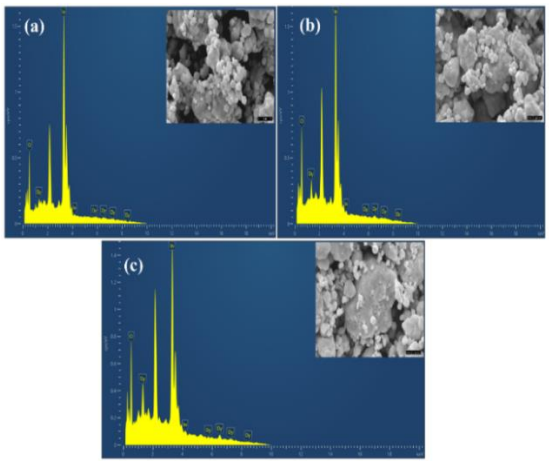


**Fig. 4** – FESEM with EDAX spectra of $(In_{1-x}Dy_x)_2O_3$ nano powders (a) $x = 0.02$, (b) $x = 0.05$, and (c) $x = 0.09$ calcined at 900 °C

**Table 2** – The atomic percentages (at. %) of $(In_{1-x}Dy_x)_2O_3$ nano powder samples from EDAX analysis

| Samples | In (at. %) | Dy (at. %) | O (at. %) | Total (at. %) |
|---|---|---|---|---|
| S-X ($x = 0.02$) | 45.59 | 2.81 | 51.60 | 100 |
| S-Y ($x = 0.05$) | 39.85 | 3.77 | 56.38 | 100 |
| S-Z ($x = 0.09$) | 35.51 | 11.13 | 53.36 | 100 |

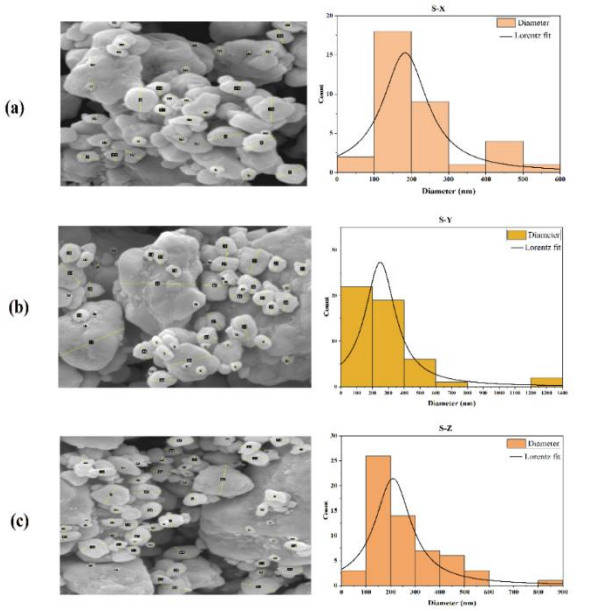


**Fig. 5** – Diameter of particle Size distribution histogram of $(In_{1-x}Dy_x)_2O_3$ nano powder samples with the concentration of (a) $x = 0.02$, (b) $x = 0.05$, and (c) $x = 0.09$

SEM images, it can be seen that grain of different sizes was formed at different Dy concentration. A grain size of 65 nm to 300 nm was observed at low Dy concentra-

tion ($x = 0.02$) and is shown in Fig. 5(a). A grain size of 60 nm to 400 nm was observed at low Dy concentration ($x = 0.05$) and is shown in Fig. 5(b). Similarly, $(In_{1-x}Dy_x)_2O_3$ nanoparticles at Dy concentration of 0.09 at.% shown a grain size in the range of 81 nm to 300 nm as shown in Fig. 5(c). But the observed grain size is higher than that of crystallite size calculated from Scherrer relation. The $(In_{1-x}Dy_x)_2O_3$ nano powder samples' FESEM images showed porous structures and particles with sizes ranging from nano to micrometres [23].

### 3.3 Optical Properties

The diffuse reflectance spectra of $(In_{1-x}Dy_x)_2O_3$ nano powder samples with different compositions are shown in Fig. 6. The spectra were recorded in the wavelength range of 300 to 1000 nm. In the visible spectrum, it was noticed that the reflectance of the samples of $(In_{1-x}Dy_x)_2O_3$ nano powder was between 70 % and 90 %. Using the Tauc's relation and Kubelka-Munk function the band gap of $(In_{1-x}Dy_x)_2O_3$ nano powder were calculated. The Kubelka-Munk function was written as $F(R) = (1 - R)^2/2R$ in terms of the variable reflectance $R$ [24].

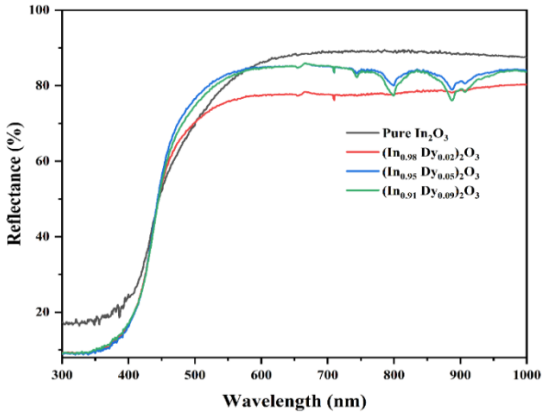


**Fig. 6** – Diffuse reflectance spectra of $(In_{1-x}Dy_x)_2O_3$ nano powder samples at $x = 0.00$, 0.02, 0.05, and 0.09

Fig. 7 depicts the band gap of pure and $(In_{1-x}Dy_x)_2O_3$ nano powders. As seen in Fig. 7, By extending the linear region of the figure of $(F(R)hv)^2$ vs. photon energy, the energy bandgap $E_g$ was calculated. The pure $In_2O_3$ powder showed a band gap of 2.89 eV, whereas Dy doped $In_2O_3$ nano powders at 2 at.%, 5 at.%, and 9 at.% of Dy showed band gaps of 2.94 eV, 2.955 eV, and 2.965 eV. In synthesized powder samples, the optical energy band gap increased from 2.94 eV to 2.96 eV when the $Dy^{3+}$ ion concentration level varied with $x = 0.02$, 0.05, and 0.09. The increase in optical band gap with increase in Dy concentration might be due to Burstein-Moss effect. As a consequence of the Fermi level migrating to the conduction band and occupying some of the bottom levels in the conduction band, the band gap increases, requiring more energy to go from the valance band to the conduction band. The spectrum shows that the absorption edge shifts towards shorter wavelengths as the concentration of dysprosium rises. It demonstrates that an increase in optical band gap was discovered, and that it was caused by the carrier concentration brought on by the inclusion of dysprosium ions and the emergence of defect levels in the energy band gap [25].

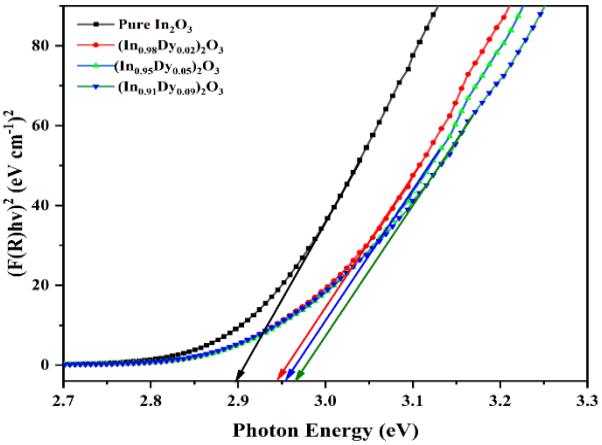


**Fig. 7** – $(F(R)hv)^2$ vs Photon energy plots of $(In_{1-x}Dy_x)_2O_3$ nano powder samples at $x = 0.00$, 0.02, 0.05, and 0.09

### 3.4 Photoluminescence Studies

Photoluminescence (PL) studies were performed for the $(In_{1-x}Dy_x)_2O_3$ ($x = 0.00$, 0.02, 0.05, and 0.09) nano powders at room temperature at an excitation wavelength of 410 nm and the spectra are shown in Fig. 8. The spectra shown that emission bands at 451 nm (Violet), 560 nm (Green), 675 nm (Red) and 784 nm. The peak intensity in prepared powder samples varied depending on the amount of dysprosium present. As the concentration of Dy ions rose from 0.00 to 0.09, the peak intensity locations in the produced samples increased. As the concentration of Dy ions rose from 0.00 to 0.09, the peak intensity locations in the produced samples increased. The peak intensities for the composition of the 2 at.% and 5 at.% were very comparable because the $Dy^{3+}$ ions in the host lattice changed so very little. Band edge recombination and imperfections cause metal oxide semiconductors cause for luminesce [26, 27].

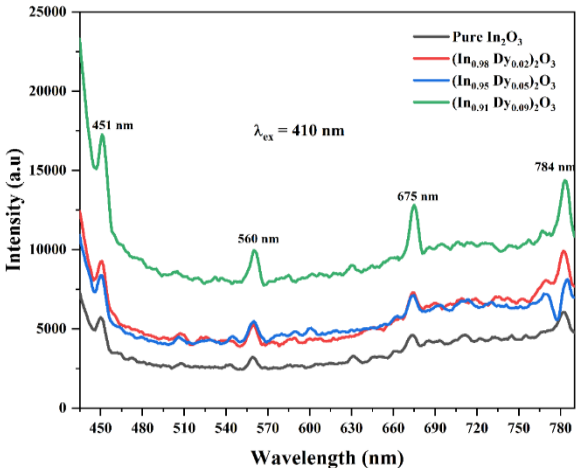


**Fig. 8** – Photoluminescence spectra of $(In_{1-x}Dy_x)_2O_3$ nano powder samples

The peak intensity varied with the concentration of Dy ions, according to Hosamani et al. [20] who stimulated the material at 325 nm and only detected the peak at 580 nm (Yellow). In general, oxygen vacancies will play an important role in inducing photolumines-

cence property. Here the oxygen vacancies might be developed by adding Dy impurity ions into the host $In_2O_3$ lattice and may cause off stoichiometry in the host material. Further, defects might also be one reason for the observed PL property in pure and Dy doped $In_2O_3$.

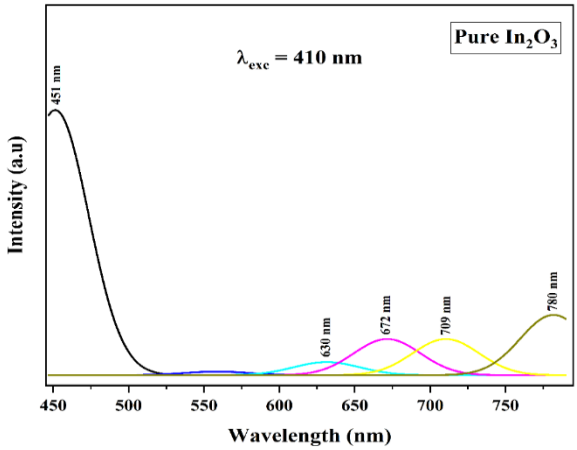


**Fig. 9** - Deconvolution of photoluminescence spectra of pure $In_2O_3$ nano powder

Fig. 9 depicts the deconvolution of pure $In_2O_3$ nano powder samples that were stimulated at 410 nm while they were at room temperature. The range of wavelengths from 440 nm to 790 nm is taken into account in the graph of intensity against wavelength that represents the photoluminescence spectrum with baseline correction. The most prominent intensity peaks could be found at 451 nm (violet), a barely noticeable intensity peak at 558 nm, and lesser intensity peaks at 630, 672, 709, and 780 nm (red region).

The incorporation of $Eu^{3+}/Dy^{3+}$ ions into the $In_2O_3$ lattice was accomplished by Dimple et al. using Sonochemical method. The sample displays very weak emission bands when stimulated at 235 nm. These bands are formed by transitions of $Eu^{3+}$ ions in the $In_2O_3$ lattice in contrast to transitions of $Eu^{3+}/Dy^{3+}$ ions. In the instance of Dy-doped $In_2O_3$, there was no emission seen. This might be because the $In_2O_3$ lattice was under a significant amount of strain around the $Dy^{3+}$ (doping) ions [28].

### 3.5 Magnetic Properties

The magnetic hysteresis loop for $(In_{1-x}Dy_x)_2O_3$ nano powders at room temperature is shown in Fig. 10 where an external magnetic field of $\pm$ 5000 G was applied. The magnetic studies were carried out at room temperature (300 K). As can be seen in Fig. 10, pure $In_2O_3$ nano powder in this condition has paramagnetic properties. With different concentrations of Dy ($x = 0$), 0.02, 0.05, and 0.09, the $(In_{1-x}Dy_x)_2O_3$ nano powders that were produced shown either a paramagnetic or a mild ferromagnetic behaviour. The strength of magnetization increased with increase of applied magnetic field and no magnetic saturation was found even at higher applied magnetic field. Similar results were also observed for Dy doped $In_2O_3$ nano powders at different Dy concentrations. Additionally, the coercivity ($H_c$ = 310.46 to 1.0651 Gauss), the saturation Magnetization ($M_s = 7.45 \times 10^{-3}$ to $111 \times 10^{-3}$ emu/g), and the retentivity ($M_r = 2.476 \times 10^{-3}$ to $20.25 \times 10^{-3}$ emu/g) all drop as the concentration of Dy ions in $In_2O_3$ rises. $(In_{1-x}Dy_x)_2O_3$ nano powders, to the best of our knowledge, display behaviours ranging from para magnetic to ferromagnetic properties.

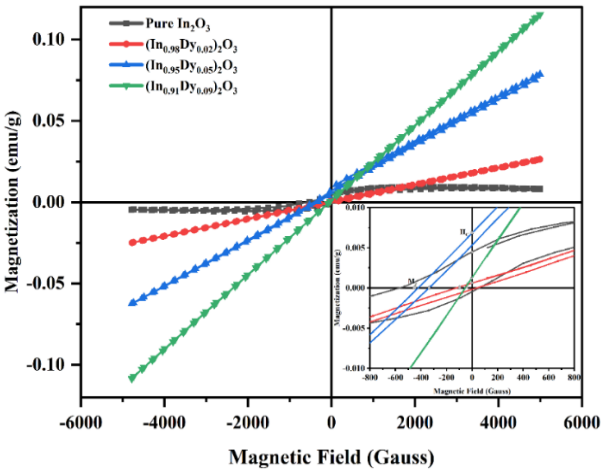


**Fig. 10** – Magnetization hysteresis curve of $(In_{1-x}Dy_x)_2O_3$ nano powders ($x$ = 0, 0.02, 0.05 and 0.09) at room temperature

When doping dysprosium ions into $In_2O_3$ to produce a magnetic nature, spin-spin interactions between dysprosium ions may be created thanks to an oxygen vacancy [2, 27, 29]. Ferromagnetism at ambient temperature in dilute magnetic semiconductors may be influenced by a wide variety of applications [30-33]. Some of these factors include oxygen vacancy, spin polarisation, lattice distortion, magnetic impurities, and ferromagnetic clusters. The $(In_{1-x}Dy_x)_2O_3$ nano powders exhibit a weak ferromagnetic behaviour owing to oxygen vacancy associated defects and short-range ferromagnetic ordering [34, 35]. Hosamani et al. [20] used an auto combustion approach to synthesize Dy doped indium oxide nanoparticles and found the evidence of modest ferromagnetism in Dy-doped indium oxide samples.

## 4. CONCLUSIONS

To summarise, $(In_{1-x}Dy_x)_2O_3$ nano powders were synthesized by solid-state reaction with $Dy^{3+}$ ions in varying concentrations ($x$ = 0.00, 0.02, 0.05, and 0.09). In order to investigate the crystallite sizes of the nano powders, X-ray diffraction technique was used. The crystallite sizes of the samples varied from 31 to 82 nm and had a cubic structure with a single phase. The lattice constant of the prepared nano powders increased from 10.06 Å to 10.22 Å. As the concentration of $Dy^{3+}$ increases, the size of the crystallites decreases, but at the same time the lattice constant increases. FESEM micrographs showed that the nanoparticles had a semi-spherical form, and EDAX analysis revealed the compositional weight percent and atomic weight percent of the selected composition. As the quantity of $Dy^{3+}$ changed, researchers found that different samples of $(In_{1-x}Dy_x)_2O_3$ nano powder had energy bandgaps that ranged anywhere from 2.89 to 2.96 eV. A rise in dopant concentration is seen in the photoluminescence spectra, which is then followed by an increase in intensity at an

excitation wavelength of 410 nm. Emission in the violet, green, and red areas may be seen in photoluminescence spectra because to the presence of oxygen vacancies and their influence. The produced $(In_{1-x}Dy_x)_2O_3$ nano powders display modest ferromagnetism at ambient temperature, while the magnetic properties of $In_2O_3$ in their natural state are para magnetic. If there is a higher concentration of $Dy^{3+}$ in the $In_2O_3$ lattice, then there will be a higher level of magnetic saturation.

## ACKNOWLEDGEMENTS

The authors acknowledge VIT- AP's financial assistance and VIT Vellore's assistance with sample characterisation. The photoluminescence spectra were provided by Dr. Abdul Azeem, an Associate Professor of Physics at NIT Warangal in India. For supplying VSM data, the authors are thankful to Dr. G.A. Basheed, a Scientist at CSIR-NPL New Delhi.

## REFERENCES

1. T. Dietl, *Nat. Mater.* **2**, 646 (2003).
2. X. Huang, A. Makmal, J.R. Chelikowsky, L. Kronik, *Phys. Rev. Lett.* **94**, 236801 (2005).
3. J.M.D. Coey, *Curr. Opin. Solid State Mater. Sci.* **10**, 83 (2006).
4. K. Wongsaprom, R. Jareanboon, S. Kingcha, S. Pinitsoontorn, W. Ponhan, *J. Supercond. Nov. Magn.* **30**, 1053 (2016).
5. S.A. Chambers, T.C. Droubay, C.M. Wang, K.M. Rosso, S.M. Heald, D.A. Schwartz, K.R. Kittilstved, D.R. Gamelin, *Mater. Today* **9**, 28 (2006).
6. M. Jothibas, C. Manoharan, S.J. Jeyakumar, P. Praveen, *J. Mater. Sci. Mater. Electron.* **26**, 9600 (2015).
7. L.M. Huang, C.M. Araujo, R. Ahuja, *Eur. Phys. Lett.* **87**, 27013 (2009).
8. W. Xu, Y. Liu, B. Chen, D.-B. Liu, Y.-H. Lin, A. Marcelli, *Phys. Chem. Chem. Phys.* **15**, 17595 (2013).
9. S. Kohiki, M. Sasaki, Y. Murakawa, K. Hori, K. Okada, H. Shimooka, T. Tajiri, H. Deguchi, S. Matsushima, M. Oku, T. Shishido, M. Arai, M. Mitome, Y. Bando, *Thin Solid Films* **505**, 122 (2006).
10. G. Kiriakidis, H. Ouacha, N. Katsarakis, *Rev. Adv. Mater. Sci.* **4**, 32 (2003).
11. K.K. Pawar, V.L. Patil, N.L. Tarwal, N.S. Harale, J.H. Kim, P.S. Patil, *J. Mater. Sci.: Mater. Electron.* **29**, 14508 (2018).
12. K. Anand, J. Kaur, R.C. Singh, R. Thangaraj, *Mater. Sci. Semicond. Proc.* **39**, 476 (2015).
13. Ram Prakash, Shalendra Kumar, Faheem Ahmed, Chan Gyu Lee, Jung Il Song, *Thin Solid Films* **519**, 8243 (2011).
14. G. Peleckis, X.L. Wang, S.X. Dou, P. Munroe, J. Ding, B. Lee, *J. Appl. Phys.* **103**, 07D113 (2008).
15. L. Xu, B. Dong, Y. Wang, X. Bai, J. Chen, Q. Liu, H. Song, *J. Phys. Chem. C* **114**, 9089 (2010).
16. Y. Wang, Y. Zhu, X. Xu, J. Huang, Z. Lu, D. Qiu, *RSC Adv.* **7**, 54500 (2017).
17. K. Anand, J. Kaur, R.C. Singh, R. Thangaraj, *Chem. Phys. Lett.* **682**, 140 (2017).
18. R. Reisfeld, C.K. Jorgensen, K.A. Gschneider, L. Eyring, *Excited State Phenomena in Vitreous Materials* in *Handbook on the Physics and Chemistry of Rare Earths*, **9**, 1-90 (*Elsevier Sci.*: 1987).
19. A. Zelati, A. Amirabadizadeh, A. Hosseini, *Int. J. Ind. Chem.* **5**, 69 (2014).
20. G. Hosamani, B.N. Jagadale, J. Manjanna, S.M. Shivaprasad, D.K. Shukla, J.S. Bhat, *J. Electron. Mater.* **50**, 52 (2021).
21. K. Anand, R. Thangaraj, N. Kohli, R.C. Singh, *AIP Conf. Proc.* **1591**, 477 (2014).
22. B. Balaraju, S. Kaleemulla, N. Madhusudhana Rao, I. Omkaram, D. Sreekantha Reddy, *Optik* **154**, 821 (2018).
23. K. Chaitanya Kumar, N. Madhusudhana Rao, S. Kaleemulla, G. Venugopal Rao, *Physica B: Condens. Matter.* **522**, 75 (2017).
24. A.A. Christy, O.M. Kvalheim, R.A. Velapoldi, *Vibrational Spectrosc.* **9** No 1, 19 (1995).
25. J. Sivasankar, P. Mallikarjuna, N. Madhusudhana Rao, S. Kaleemulla, M. Rigana Begam, G. Venugopal Rao, *Mech. Mater. Sci. Eng*, 188, (2017).
26. Y. Li, Y. Bando, D. Golberg, *Adv. Mater.* **15**, 581 (2003).
27. P.K. Sharma, R.K. Dutta, R.J. Choudhary, A.C. Pandey, *CrystEngComm* **15**, 4438 (2013).
28. Dimple P. Dutta, V. Sudarsan, P. Srinivasu, A. Vinu, A.K. Tyagi, *J. Phys. Chem. C* **112**, 6781 (2008).
29. Y. An, Y. Xing, F. Pan, Z. Wu, J. Liu, *Phys. Chem. Chem. Phys.* **18**, 13701 (2016).
30. G. Dascalu, T. Popescu, M. Feder, O.F. Caltun, *J. Magn. Magn. Mater.* **333**, 69 (2013).
31. D. Yang, Y. An, S. Wang, Z. Wu, J. Liu, *RSC Adv.* **4**, 33680 (2014).
32. J. Yin, F. Xu, H. Qu, C. Li, S. Liu, L. Liu, Y. Shao, *Phys. Chem. Chem. Phys.* **21**, 11883 (2019).
33. S. Kumar, S. Mukherjee, R. Kr. Singh, S. Chatterjee, A.K. Ghosh, *J. Appl. Phys.* **110**, 103508 (2011).
34. A. Singhal, S.N. Achary, J. Manjanna, O.D. Jayakumar, R.M. Kadam, A.K. Tyagi, *J. Phys. Chem. C.* **113**, 3600 (2009).
35. A. Singhal, S.N. Achary, J. Manjanna, S. Chatterjee, P. Ayyub, A.K. Tyagi, *J. Phys. Chem. C* **114**, 3422 (2010).

## Комплексне дослідження оптичних і магнітних властивостей нанопорошків $(In_{1-x}Dy_x)_2O_3$, отриманих методом твердофазної реакції

Lakshmi Rajesh Chebrolu[1], Madhusudhana Rao Nasina[1], Kaleemulla Shaik[2], Maddikera Kalyan Chakravarthi[3]

[1] *Department of Physics, School of Advanced Sciences, VIT-AP University, Amaravati, 522237 Andhra Pradesh, India*
[2] *Thin Films Laboratory, Centre for Functional Materials, Vellore Institute of Technology, Vellore, 632014 Tamil Nadu, India*
[3] *School of Electronics Engineering, VIT-AP University, Amaravati, 522237 Andhra Pradesh, India*

У цьому дослідженні наночастинки $In_2O_3$, леговані Dy, були синтезовані за допомогою твердофазної реакції з різними концентраціями: 2; 5 і 9 ат.%. На основі досліджень рентгенівської дифракції було встановлено, що зразки порошку мають кубічну кристалічну структуру біксбіїту та розміри крис-

талітів 31-82 нм. Методом скануючої електронної мікроскопії установлені розміри зерен 100-300 нм. Енергодисперсійний аналіз рентгенівських спектрів (EDAX) показав, що синтезовані наночастинки не містять домішок. Використовуючи спектри дифузного відбиття, було розраховано оптичну ширину забороненої зони, яка зростала від 2,89 до 2,96 еВ зі збільшенням концентрації іонів $Dy^{3+}$. Спектри фотолюмінесценції показали піки випромінювання у видимій області спектра, коли зразки збуджувалися джерелом світла з довжиною хвилі 410 нм. При температурі навколишнього середовища чистий $In_2O_3$ виявляв парамагнітну природу, тоді як наночастинки $(In_{1-x}Dy_x)_2O_3$ були феромагнітними.

**Ключові слова:** Оксид індія, Оксид диспрозію, Рідкоземельні оксиди, Фотолюмінесценція, Вібраційний магнітометр.